Numerical Modeling and Analysis of Dynamic Crack Propagation in Rubber

Elsiddig Elmukashfi[1,*], Martin Kroon[1]

[1] Department of Solid Mechanics, Royal Institute of Technology, Osquars backe 1,
SE-100 44 Stockholm, Sweden
* Corresponding author: elsiddig@kth.se

Abstract Dynamic crack propagation in rubber is modeled and analyzed numerically using the finite element method. The problem of a suddenly initiated crack at the center of stretched sheet is studied under plane stress conditions. A nonlinear finite element analysis using implicit time integration scheme is used. The bulk material behavior is described by finite-viscoelasticity theory and the fracture separation process is characterized using a cohesive zone model with a bilinear traction-separation law. Hence, the numerical model is able to model and predict the different contributions to the fracture toughness, i.e. the surface energy, viscoelastic dissipation, and inertia effects. The separation work per unit area and the cohesive strength has been parameterized, and their influence on the separation process has been investigated. A steadily propagating crack is obtained and the corresponding crack tip position and velocity history as well as the steady crack propagation velocity are evaluated and compared with the experimental data. A minimum threshold stretch of 3.0 is required for crack propagation. The numerical model is able to predict the dynamic crack growth such that the strength and the surface energy vary with the crack speed.

Keywords rubber, crack, viscoelasticity, cohesive zone, dynamic fracture

1. Introduction

Elastomers are important materials in many engineering applications; consequently a wide variety of elastomeric materials is used in several products, e.g., tires, springs, dampers, gaskets, bearings, oil seals, etc. Fracture mechanics in elastomers is of great importance in the design process and it is fundamental in some applications such as adhesion technology, elastomers wear, etc.

Dynamic crack propagation in rubber-like materials has been investigated both theoretically and experimentally but the field is relatively undeveloped compared with brittle materials [8, 12, 21, 28]. Generally, the dynamic fracture in rubber shows remarkable deviation from the dynamic fracture theories for brittle materials, e.g. the cracks propagate at speeds greater than the speed of sound without branching and at high stretch levels oscillatory crack propagation results.

The fracture energy of rubber is the sum of different contributions [20, 22, 23]: the surface energy required to create new crack surfaces, the energy dissipated in the viscoelastic processes around the crack tip, and the inertia effects that contribute in the case of dynamic fracture. Furthermore, the separation process is accompanied with a viscoelastic dissipation process to which takes place in the crack tip vicinity [2].

The theoretical treatment of the problem of crack propagation in rubber-like solid reveals that the region around the crack tip can be divided into three different zones, determined by the relaxation spectrum, as shown in Fig. 1a [10]. These regions are: glassy region occurs at the closest to the crack tip, rubbery region occurs far from the crack tip, the viscous dissipation region that is located between these two regions. Depending on the relaxation spectrum and crack propagation velocity, the glassy and viscous dissipation regions may vanish, e.g. in the case of carbon-filled natural rubber glassy zones are not expected to exist, while viscous dissipation is expected.
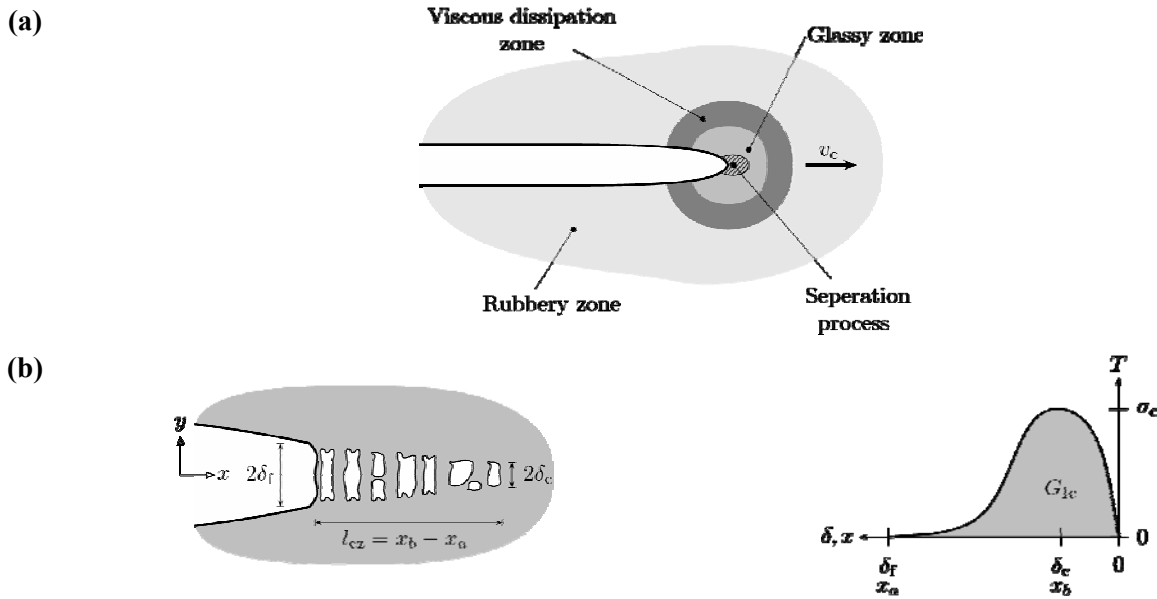
(a)

(b)

Figure 1. The fracture processes around a crack propagating in rubber with a speed v_c: **a** the different zones around the propagating crack tip determined by the viscoelastic behavior; and **b** the cohesive process zone and its traction-separation law ($T - \delta$). G_{Ic} is the fracture energy, l_{cz} is the length of the cohesive zone, δ_c is the critical displacement, δ_f is the failure displacement, and σ_c is the cohesive strength.

One way to give a quantitative description of the contribution from the different fracture-associated processes is to use the cohesive zone theories. The cohesive zone modeling approach was originally proposed by Dugdale and Barenblatt [9, 11] to simulate the fracture process and was later implemented in a finite element environment [3]. A cohesive zone model describes the fracture process in the crack tip vicinity as a gradual surface separation process, such that the normal and shear forces at the interface resist separation and relative sliding. Several cohesive zone models have been introduced in the literature including rate-dependent and independent models and have been successfully used in both quasi-static and dynamic crack growth problems [1, 4, 13, 27].

The purpose of the present study is to model as well as to analyze the dynamic crack propagation in rubber. The problem of a suddenly initiated crack at the center of stretched sheet is analyzed using finite element method, and plane stress conditions are assumed to prevail. A nonlinear finite element analysis using implicit time integration scheme is used. The bulk material behavior is described by finite-viscoelasticity theory. The fracture separation process is modeled using a cohesive zone model with a bilinear traction-separation law. A parametric study is performed over a range of cohesive zone properties, i.e. cohesive strength and energy, and the steady crack propagation velocity is calculated and compared with crack speeds obtained in experiments. The problem is formulated in Section 2, and the numerical analysis is provided in Section 3. A discussion is presented in Section 4.

2. Problem formulation

2.1. Geometry

Consider a thin rectangular sheet of rubber with the initial dimensions $2W_0$ (width), $2H_0$ (height), and B_0 (thickness), as shown in Fig. 2a. The sheet is initially unloaded, and the Cartesian material coordinates X_I, $I = 1,2,3$, are used to describe the reference configuration. Plane stress conditions are assumed to prevail, such that the $X_1 - X_2$-plane is the plane of stresses. The sheet is first subjected to a stretch λ in the X_2-direction at low rate of loading, such that inertia effects are

ignored. The deformation is assumed to be defined by the motion $\mathbf{x} = \chi(\mathbf{X}, t)$, where the Cartesian coordinates x_i, $i = 1,2,3$, are defined in the deformed configuration, as shown in Fig. 2b. The position vectors in material and spatial coordinates are defined as $\mathbf{X} = X_i \mathbf{e}_i$ and $\mathbf{x} = x_i \mathbf{e}_i$, respectively, such that the two coordinates possess the same origin and the same set of orthogonal basis vectors $\mathbf{e}_i$, $i = 1,2,3$. The displacement vector is defined as $\mathbf{u} = \mathbf{x} - \mathbf{X}$, and the first Piola-Kirchhoff traction vector $\mathbf{T}$ is defined as force per unit undeformed area. After the required extension has been achieved, a crack of length $2a$ is initiated at the center of the deformed sheet parallel to x_1-direction. Thereafter, the crack propagates dynamically and symmetrically along a path defined by $x_2 = 0$.

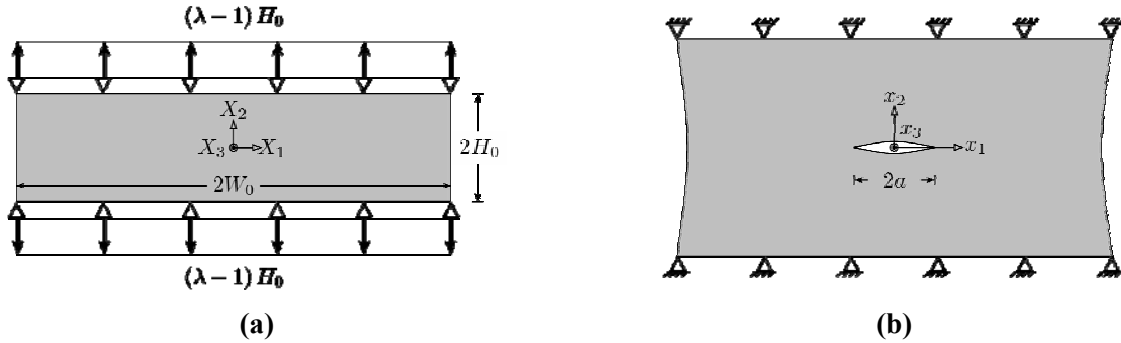(a)   (b)

Figure 2. The geometry of the thin rectangular rubber sheet: **a** the reference configuration; and **b** the current configuration.

Considering the symmetry of loading and geometry, only a half portion of the sheet, defined by $X_1 \geq 0$, is modeled. The crack propagation is then studied over a length of Δa in the deformed configuration. The time scale is defined according to the following: the sheet is loaded quasi-statically for $t < 0$, and at $t = 0$, the crack is initiated. The boundary conditions applied for the whole period of time are defined according to

$$X_1 = 0 : u_1 = 0, T_2 = 0, \tag{1}$$

$$X_1 = W_0 : T_1 = T_2 = 0, \tag{2}$$

$$X_2 = \pm H_0 : u_1 = 0, u_2 = \pm(\lambda - 1) \cdot H_0. \tag{3}$$

The initial crack is located at $0 \leq X_1 \leq a_0$, $X_2 = 0$. Note that a pertains to the deformed configuration, while a_0 pertains to the reference configuration. The crack starts to propagate immediately after the initiation process, i.e. for $t > 0$. The propagation process is determined by a cohesive law. Assuming that the crack tip position is defined as $\mathbf{x}_{tip} = x_{tip} \mathbf{e}_1$, the crack tip velocity is then determined as

$$v_{tip} = \frac{dx_{tip}}{dt}, \tag{4}$$

implying that the crack propagates in the X_1-direction, i.e. $\mathbf{v}_{tip} = v_{tip} \mathbf{e}_1$ and d/dt is the time derivative taken with respect to spatial coordinates.

2.2. Constitutive models

2.2.1. The finite-strain viscoelasticity model

The mechanical behavior of rubber-like materials is characterized by finite elasticity theory, i.e. hyperelasticity, for the quasi-static response. Further, the dynamic response is often characterized by viscoelasticity theory. The finite-strain viscoelasticity implementation in ABAQUS [14] is based on a local additive split of the stress tensor into initial and non-equilibrium parts [15]. The initial part

follows the finite-strain constitutive equations while the non-equilibrium part determines the viscous response.

Consider a deformation that is defined by the deformation gradient $\mathbf{F}$ and the associated Jacobian J. The deformation gradient is decomposed into volume changing (dilatational) part $J^{2/3}\mathbf{I}$ and volume preserving (distortional) part $\overline{\mathbf{F}} = J^{1/3}\mathbf{F}$. The initial free strain energy function, that determines the initial stress part, can be written in the decoupled form

$$\Psi = \Psi_{vol}(J) + \Psi_{iso}(\overline{\mathbf{F}}), \qquad (5)$$

where $\Psi_{vol}(J)$ is the volumetric part and $\Psi_{iso}(\overline{\mathbf{F}})$ is the isochoric part. The total strain energy, including the viscous response, can be written using a generalized Maxwell model (Prony series) as

$$\Psi = k_R(t) \cdot \Psi_{vol}(J) + g_R(t) \cdot \Psi_{iso}(\overline{\mathbf{F}}), \qquad (6)$$

where $k_R(t)$ and $g_R(t)$ are the Prony series dimensionless relaxation moduli.

In this context, an isotropic and incompressible hyperelastic material is considered, i.e. $J = 1$. Hence, the volumetric part of the strain energy function is then expressed in terms of a hydrostatic pressure p.

$$\Psi_{vol} = p(J - 1), \qquad (7)$$

The isochoric part of the strain energy function is defined by the Ogden model for incompressible materials [25], which reads

$$\Psi_{iso} = \sum_{p=1}^{M} \frac{\mu_p}{\alpha_p}\left(\lambda_1^{\alpha_p} + \lambda_2^{\alpha_p} + \lambda_3^{\alpha_p} - 3\right), \qquad (8)$$

where the λ_i, $i = 1,2,3$, are the principal stretches, μ_p and α_p are material parameters that fulfill the condition $\mu_p \alpha_p > 0$ (no summation) and the shear modulus μ_p is defined by $\mu = \sum_{p=1}^{M} \mu_p \alpha_p$.

Further, the volumetric response is assumed to be purely elastic such that the viscoelastic response is determined by the isochoric response, i.e. $k_R(t) = 1$. The total strain energy function, including the viscoelastic response, can be written in the decoupled form

$$g_R(t) = 1 - \sum_{i=1}^{N} \overline{g}_i^P\left(1 - e^{-t/\tau_i}\right), \qquad (9)$$

where N, $\overline{k}_i^P$, $\overline{g}_i^P$ and τ_i are material constants. The model includes N Maxwell elements, i.e. series combinations of spring and dash-pot.

2.2.2. The cohesive zone model

The constitutive response for the cohesive surface is modeled in terms of the relationship between the traction and the displacement jump across the surface. The traction-separation law (TSL) is a physically based or a phenomenological model that can be obtained from a free energy density function, ϕ, as

$$\mathbf{T} = \mathbf{T}(\mathbf{\Delta}) = \frac{\partial \phi}{\partial \mathbf{\Delta}}, \qquad (10)$$

where $\mathbf{T}$ is a first Piola-Kirchhoff traction vector, and $\mathbf{\Delta}$ is the displacement jump vector between two initially coincident points which are defined in three different directions the normal (n) direction, and the two shear directions (s and t) with respect to the cohesive surface.

In this work, a bilinear traction-separation law is used, and only the opening mode fracture (mode I) is considered. For this reason, only the constitutive behavior in the normal direction is controlled, see Fig. 3. The material parameters of the bilinear traction-separation law are K_n (the initial elastic

or penalty stiffness), δ_n^c (the critical normal separation), δ_n^f (the failure separation), and σ_c (the cohesive strength in the normal direction).
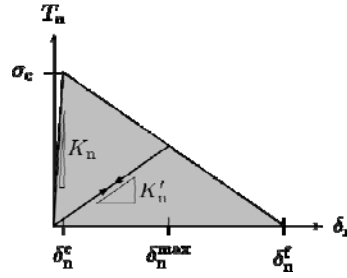

Figure 3. The bilinear traction-separation law

The cohesive element behavior in ABAQUS [14] is based on the characterization of the damage process as the degradation of the material stiffness. The initial behavior is assumed to be linear elastic and is active until damage is initiated. When damage is initiated, the material stiffness decreases and the rate of degradation is defined by the damage evolution law. A scalar damage variable, d, that determines the stiffness degradation, is used, which evolves monotonically from 0 to 1, i.e. from an undamaged to a fully damaged state. The irreversible bilinear traction-separation law is then written as

$$T_n = \begin{cases} K_n \delta_n & \text{if } \delta_n \leq \delta_n^c, \\ (1-d)\cdot K_n \delta_n & \text{if } \delta_n \geq \delta_n^c, \end{cases} \tag{11}$$

where the linear elastic unloading behavior after damage onset is determined by the degraded stiffness $K_n' = (1-d)\cdot K_n$. The damage variable, d, for linear softening is determined as

$$d = \frac{\delta_n^f \left(\delta_n^{max} - \delta_n^c\right)}{\delta_n^{max} \left(\delta_n^f - \delta_n^c\right)}, \tag{12}$$

where δ_n^{max} is the maximum value of the displacement attained during the loading history, see Fig. 3. A maximum nominal stress criterion is used to predict damage initiation, i.e. damage is assumed to be initiated when the maximum nominal stress reaches a critical level $T_n \geq \sigma_c$.

3. Numerical analysis

3.1 Estimation of material parameters

A carbon-black-filled natural rubber material is considered here and its physical and chemical properties are illustrated in [5, 10]. This material has been studied extensively [5-7].
Experimental data from a uniaxial tensile test for the carbon-black filled natural rubber [3] has been used to estimate the parameters in the Ogden strain energy function. The Cauchy (true) stress, σ, in the uniaxial test is defined by

$$\sigma = \sum_{p=1}^{M} \mu_p \left(\lambda^{\alpha_p} - \lambda^{-(1/2)\alpha_p}\right), \tag{13}$$

where λ is the stretch in the uniaxial tension direction. Using a nonlinear least squares method, the Cauchy stress in Eq. (13) is fitted to the uniaxial tension data and two sets of parameters are found to be sufficient, see Fig. 3. The parameter values are shown in Table 1.

Table 1. The Ogden strain energy function parameters ($M = 2$)

p	μ_p [MPa]	α_p [-]
1	1.639	2.724
2	0.088	0.004

Free retraction test experimental data [5] is used to estimate the model parameters in the

viscoelasticity model. Maxwell model with one element has been used, i.e. $N = 1$. The relaxation time for rubber is experimentally found to be of the order of $1.0\,\mathrm{s}$ at ambient temperatures [19, 26], and therefore we assumed a relaxation time of $\tau_1 = 1.0\,\mathrm{s}$. (The viscoelastic response of the rubber material is much slower than the rapid processes that we are considering in the present dynamic crack propagation analysis, so the exact value of τ_1 is irrelevant.) The associated relative stiffness, g_1^p, then has to be determined from the experimental data from the retraction tests.
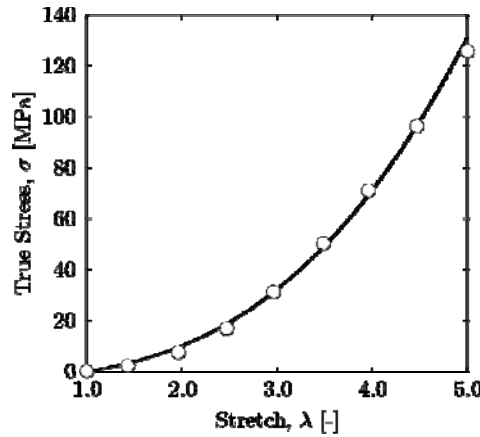

Figure 4. Comparison between the uniaxial true stress-stretch data ('$\circ$') [5] and Ogden material model ($M = 2$)

In the free retraction experiment, we consider a thin rectangular strip of rubber with initial dimensions $L_1 = 250\,\mathrm{mm}$, $L_2 = 10\,\mathrm{mm}$ and $L_3 = 0.5\,\mathrm{mm}$, see Fig. 5a (i). The strip is stretched quasi-statically to a certain stretch, λ_0, and then one end is released as shown in Fig. 5a (ii). Consequently, the released end undergoes retraction at a relatively high speed which depends on the initially imposed stretch as well as the material parameters.
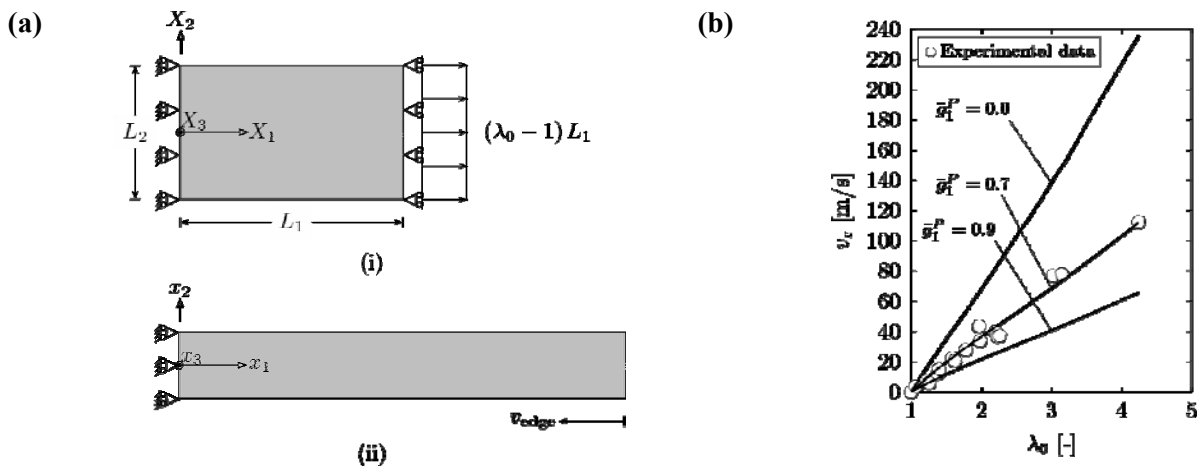

Figure 5. The free retraction experiment: **a** the geometry of the rubber specimen used in the free retraction experiments (i) the reference configuration; and (ii) the current configuration; **b** the predicted retraction speeds for different viscoelastic properties compared with the experimental data [7]. The dashed, full, and dotted lines represent different values of the relative stiffness ($g_1^P = 0.0, 0.7$, and 0.9), respectively.

The initial-boundary value problem for the free retraction experiment is analyzed using a two-dimensional plane stress finite element model. A nonlinear dynamic analysis, using an implicit time integration scheme, is performed using the finite element code ABAQUS [14], and the free edge steady retraction velocity, v_r, is computed and fitted to the data from the retraction velocity tests, see Fig. 5(b) using different values of the relative stiffness, g_1^P. The parameter values obtained for the Maxwell model are shown in Table 2 below.

Table 2. Prony series coefficients

i	$\bar{g}_i^P$	τ_i
1	0.7	1.0

3.2 Numerical implementation

The initial-boundary value problem described in Sec. 2 is numerically solved using the finite element code ABAQUS [14]. A nonlinear quasi-static analysis is used for the initial loading, and a nonlinear dynamic analysis, using implicit time integration, is used for the crack propagation analysis.

The rubber material is modeled using finite-strain viscoelasticity as described in Sec. 2.2.1 and the material parameters in Tables 1 and 2 are used.

The fracture separation process is modeled using the cohesive zone model that is described in Sec. 2.2.2. The cohesive zone parameters, the cohesive strength and cohesive energy, are material parameters that determine the length of the process zone together with the other material properties [3, 17]. They are not easily measurable, and they are often estimated using experimental data of a known problem setup. The cohesive strength is directly related to the tensile strength of the material while the cohesive energy may be estimated on the basis of fracture mechanics experiments as the work needed for fracture. However, in such estimates, both the actual surface energy and additional dissipative work are included. In this work the cohesive energy is equal is assumed to be total fracture energy. The cohesive strength is chosen to be $\sigma_c = 30\,\text{MPa}$ and then the experimental data are fitted using variable fracture energy.

A high value of the initial stiffness K_n is often assumed in order to avoid ill-conditioning and to reduce the changes of the structure compliance due to the presence of the compliance of the cohesive elements. Therefore, the initial stiffness is assumed to be $K_n = 2.67 \times 10^6\,\text{MPa}$ such that a stiff behavior is obtained prior to damage initiation without risking the numerical instabilities.

The geometry of the thin rectangular sheet in Fig. 2 is discretized, and a typical finite element mesh is shown in Fig. 6. Due to symmetry, only one half of the specimen is analyzed. The initial dimensions are taken as $W_0 = 75\,\text{mm}$, $H_0 = 5\,\text{mm}$, and $B_0 = 0.5\,\text{mm}$ [6]. The initial crack is assumed to be $2a_0 = 10\,\text{mm}$, and the crack propagation is studied over a length of $\Delta a = 50\,\text{mm}$. Note that Δa pertains to the deformed configuration, while Δa_0 pertains to the reference configuration. The 4-node bilinear plane stress element CPS4 and 4-node two-dimensional linear cohesive element COH2D4 are used in the discretisation. The cohesive elements are inserted along the crack propagation path, i.e. along $X_2 = 0$, and the bulk elements are defined elsewhere. The top and bottom faces of the cohesive elements are tied to the adjacent bulk plane stress elements, implying that three cohesive elements are attached to two bulk elements, see Fig. 6b. The cohesive elements are modeled with zero initial thickness in the reference configuration, and consequently the top and bottom faces and nodes coincide. The mesh comprises 27207 elements, of which 25506 are bulk elements and 1701 are cohesive elements. A cohesive element length of $l_{ce} = 0.025\,\text{mm}$ is used.

The element death/birth technique is adopted to model crack initiation. The initial crack domain is discetized using cohesive elements, and therefore they have been removed at the instant of crack initiation, i.e. at $t = 0$.

The problem is solved for different values of the initial stretching, i.e. $\lambda = [2.0, 4.0]$. The relative normal separation displacement, Δu_2, between each pair of initially coincident nodes in the interface ($X_2 = 0$) is computed and recorded during the analysis. The crack tip position, x_{tip}, is

defined by $\Delta u_2 = \delta_n^c$, and the crack tip velocity is determined using forward differencing of Eq. (14) of the smoothed cohesive crack tip position data, $\bar{x}_{tip}$, (using Savitzky-Golay smoothing filter).

$$v_{tip}^n = \frac{\bar{x}_{tip}^{n+1} - \bar{x}_{tip}^n}{\Delta t_n}, \tag{14}$$

where indices n and $n+1$ denote variable values at time instants t_n and t_{n+1}, respectively, and $\Delta t_n = t_{n+1} - t_n$ is the time increment. Further, the steady crack velocity, v_c, is computed by taking the average velocity over the steady propagation period.
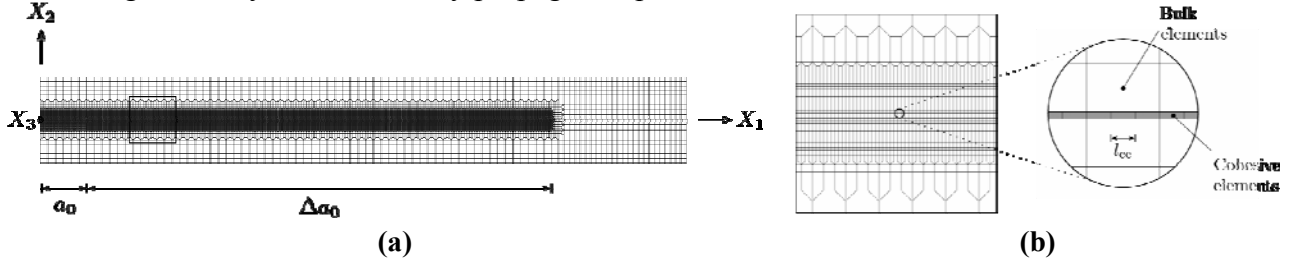

(a)   (b)

Figure 6. The finite element mesh of the thin rectangular sheet of rubber: **a** the mesh of the whole geometry; and **b** mesh details along the middle of the sheet where the cohesive elements are inserted along the crack propagation path

3.3 Numerical results

Several analyses have been performed for different combinations of stretch and cohesive zone properties. The cohesive crack tip position and velocity, as well as the steady crack propagation velocity, have been obtained for all the combinations.

Typical crack propagation results, including the cohesive crack tip position and velocity results, are shown in Figs. 8a and 8b. At $t = 0$, the crack is initiated such that it propagates immediately after the initiation, i.e. typically within less than $1\,\text{ms}$, at low velocity and continues propagating with a slow acceleration, see in Fig. 8b. After approximately $1.5\,\text{ms}$, the crack velocity approaches a transition region wherein the crack starts to accelerate rapidly and the velocity increases to high velocity levels. Then, after about $1.83\,\text{ms}$, the crack tip velocity reaches a plateau region, where steady crack propagation occurs. Different cohesive properties virtually yield the same type of behavior. Stationary crack propagation was obtained for all sets of cohesive properties, provided that the crack was able to get started. There was a threshold stretch, λ_{th}, below which the initial crack was immediately arrested and no propagation occurred.
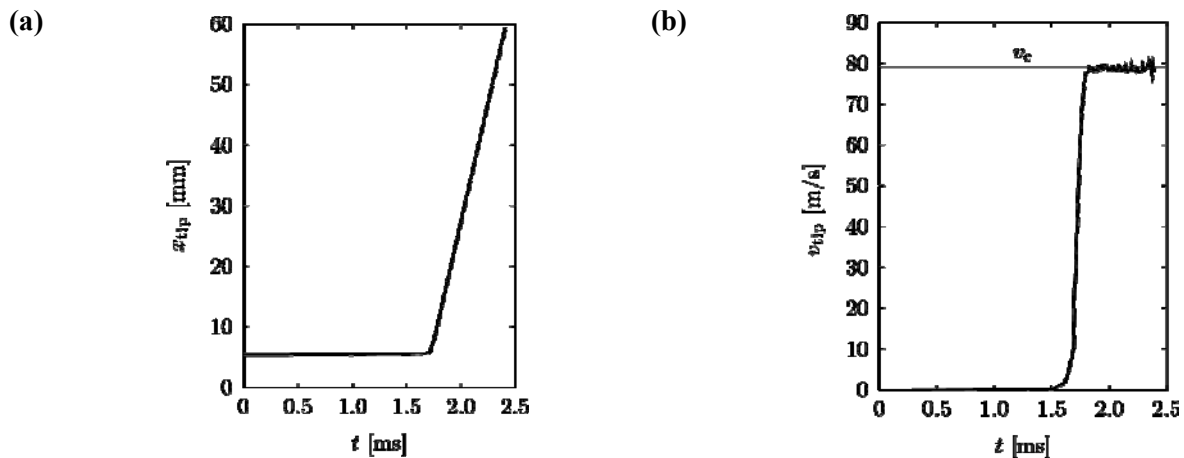

Figure 8. Crack propagation results for $\lambda = 4.0$, $\sigma_c = 60\,\text{MPa}$ and $G_{Ic} = 20\,\text{KJ/m}^2$: **a** crack tip position x_{tip} vs time t; and **b** crack tip velocity v_{tip} vs time t.

The numerical predictions of the steady crack propagation velocity are compared with the experimental data [6], as shown in Fig. 9. The numerical threshold stretch differs for the different cohesive properties, such that its minimum value, $\lambda_{th} = 3.0$, occurs for $\sigma_c = 60\,\text{MPa}$ and $G_{Ic} = 20\,\text{KJ/m}^2$. For low stretches, the model clearly overestimates the crack speeds from the experimental data. However, by using different cohesive properties, the numerical model is able to predict the crack speeds from the experiments, at least in the high stretch regime ($\lambda \geq 3.5$).
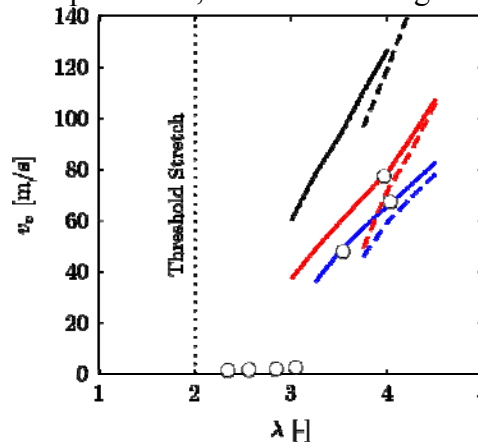

Figure 9. Comparison between numerical predictions of the steady crack propagation velocity and experimental data ('o') [4]. The black, red and blue lines indicate simulations with the cohesive strengths $30, 60, 90\,\text{MPa}$, respectively, and the full and dashed lines indicate simulations with cohesive energies $20, 40\,\text{KJ/m}^2$, respectively.

4. Discussion and concluding remarks

In the present analysis, the contribution from viscoelastic dissipation in the bulk material to the total work of fracture is negligible. This is due to the fact that the crack propagation process is very rapid in comparison with the relaxation time of the rubber material.

In the analyses, the main properties of the cohesive law, i.e. the cohesive energy and the cohesive strength, were varied to enable a prediction of the experimentally obtained crack speeds. The analyses indicate that the effective fracture energy of the rubber material at hand is to be found roughly in the range $20 - 40\,\text{KJ/m}^2$, and the cohesive strength is expected to be approximately $30 - 90\,\text{MPa}$. We emphasize that this estimate of the fracture energy should not be taken as the actual surface energy required to create new crack surface at the very crack tip. Rather, this estimate should be taken as a value that contains the actual surface energy but also significant amounts of dissipation associated with damage processes in the vicinity of the crack tip. Strictly speaking, this would be dissipation that takes place in the bulk material surrounding the crack tip, which is not really accounted for by the continuum viscoelasticity model adopted for the bulk behavior.

Few experimental investigations have been concerned with characterization of high speed fracture of rubber, in which crack speed variation with fracture toughness has been experimentally measured under high strain or loading rate. Typical fracture toughness has been reported to be in the range $7 - 300\,\text{KJ/m}^2$ for the crack speed in the range $0.5 - 30\,\text{m/s}$ using pure shear and tensile strip specimens [12, 24]. It is also shown that a low fracture toughness of $30\,\text{KJ/m}^2$ can be measured at a crack speed of $30\,\text{m/s}$. Thus, the effective fracture energy reported in the literature shows good agreement with the values attained here.

References
[1] A Corigliano, M Ricci, Rate-dependent interface models: formulation and numerical applications. Int J Solids Struct, 38(2001) 547–76.

[2] AG Thomas, The development of fracture mechanics for elastomers. Rubber Chem Technol, 67(1994) G50–G60.

[3] A Hillerborg, M Modeer and PE Petersson, Analysis of crack formation and crack growth in concrete by means of fracture mechanics and finite elements. Cem Concr Res, 6(1976) 773–81.

[4] A Needleman, A continuum model for void nucleation by inclusion debonding. J Appl Mech, 54(1987) 525–531.

[5] AN Gent, HJ Kim, Tear strength of stretched rubber. Rubber Chem Technol, 51(1978) 35–44.

[6] AN Gent, P Marteny, Crack velocities in natural rubber. J Mat Sci, 17(1982) 2955–2960.

[7] AN Gent, P Marteny, The effect of strain upon the velocity of sound and the velocity of free retraction for natural rubber. J Appl Phys, 53 (1982) 6069–6074.

[8] CH Chen, HP Zhang, J Niemczura, K Ravi-Chandar, M Marder, Scaling of crack propagation in rubber sheets. EPL 96(2011) 36009

[9] DS Dugdale, Yielding of steel sheets containing slits. J Mech Phys Solids, 8(1960) 100–4.

[10] E Elmukashfi, M Kroon, Numerical analysis of dynamic crack propagation in rubber. Int J Fract, 177 (2012) 163–178.

[11] GI Barenblatt, The mathematical theory of equilibrium cracks in brittle fracture. Adv Appl Mech, 7(1962) 55–129.

[12] GJ Lake, CC Lawrence, AG Thomas, High-speed fracture of elastomers: Part I. Rubber Chem Technol, 73(2000) 801–817.

[13] GT Camacho and M Ortiz, Computational Modeling of Impact Damage in Brittle Materials. Int. J. Solids Struct., 33(1996) 2899–2938.

[14] Hibbit, Karlsson and Sorensen Abaqus: Theory and User's Manual. Inc., Pawtucket, RI, 2011.

[15] J.C. Simo, On a Fully Three-Dimensional Finite-Strain Viscoelastic Damage Model: Formulation and Computational Aspects. Comput Method Appl M, 60 (1987) 153–173.

[16] JD Ferry, RG Mancke, E Maekawa, Y Oyanagi, and RA Dickie, Dynamic Mechanical Properties of Cross-Linked Rubbers. I. Effects of Cross-Link Spacing in Natural Rubber. J. Phys. Chem., 68(1964) 3414–3418.

[17] JR Rice, Mathematical Analysis in the Mechanics of Fracture, in Fracture: An Advanced Treatise. H. Liebowitz, ed., Vol.2 (1968) 191–311.

[18] JR Rice, Mechanics of quasi-static crack growth. In: Proceedings of Eighth U.S. National Congress on Mechanics, (1978) 191–216.

[19] JS Bergström, MC Boyce, Constitutive modeling of the large strain time-dependent behavior of elastomers. J Mech Phys solids, 46 (1998) 931–954.

[20] PG de Gennes, Soft adhesives. Langmuir, 12(1996) 4497–4500.

[21] PJ Petersan, RD Deegan, M Marder, HL Swinney, Cracks in rubber under tension exceed the shear wave speed. Phys Rev Lett, 93(2004) 1–4.

[22] PNJ Persson, O Albohr, G Heinrich, H Ueba, Crack propagation in rubber-like materials. J Phys: Condens Matter, 17(2005) R1071–R1142.

[23] M Kroon, Steady-state Crack Growth in Rubber-like Solids. Int J Fract., 169 (2011)49–60.

[24] MS Hoo Fatt, L Chen, and AA Al-Quraishi, Fracture Parameters for Natural Rubber Under Dynamic Loading. Strain 47(2011) 505–518.

[25] RW Ogden, Large Deformation Isotropic Elasticity - On the Correlation of Theory and Experiment for Incompressible Rubberlike Solids, Proceedings of the Royal Society of London, Series A, Mathematical and Physical Sciences, 326(1972) 565–584.

[26] S Kawabata, H Kawai, Strain energy density functions of rubber vulcanizates from biaxial extension. Adv. Polym. Sci., 24 (1977) 89–124.

[27] V Tvergaard, Effect of fibre debonding in a whisker-reinforced metal. Mater Sci Engng, A 125(1990) 203–213.

[28] W Wang, Hyperelasticity, viscoelasticity, and nonlocal elasticity govern dynamic fracture in rubber. Phys Rev Lett, 95(2005) 1–4.